



Journal of Semiconductors, 2024, 45 (11): 24050029, Published Online: Dec. 23, 2024

Copy Citation Text

Follow This Article

Chalcogenide perovskites—challenges, status, and future prospects



Get PDF



Full Text



图表



论文大纲



Metrics



More

Pidugu Kesavan Kannan^{1,*} Mariappan Anandkumar² Gopal Bhavani¹

chalcogenide perovskites

BaZrS₃

synthesis and DFT

OAI 2.0

AI Video Guide

AI Picture Guide

AI One Sentence

AI Short Abstract

Note: This section is automatically generated by AI . The website and platform operators shall not be liable for any commercial or legal consequences arising from your use of AI generated content on this website. Please be aware of this.

Abstract

Perovskites dominate the photovoltaic research community over the last two decades due to its very high absorption coefficient, electron and hole mobility. However, most of the reported solar cells constitute organic perovskites which offer very high efficiency but are highly unstable. Chalcogenide perovskites like BaZrS₃, CaZrS₃, etc. promise to be a perfect alternate owing to its high stability and mobilities. But, till now no stable photovoltaic device has been successfully fabricated using these materials and the existing challenges present in the synthesis of such perovskites are discussed. Also, the basic thermodynamic aspects that are essential for formation of BaZrS₃ are discussed. An extensive review on the precedent literatures—and the future direction in the BaZrS₃ photovoltaic device research is clearly given.

AI Voice

1 Introduction

In the past decade, perovskites have taken over the photovoltaic (PV) research sector, which lead to the dramatic increase of its efficiency to 25.7% over a period of 10 years. Perovskites, which are combination of organic and

inorganic halides existing in the perovskite crystal structure. Such structures exhibited very high absorption coefficient and very high electron and hole mobility^[1]. These features make these materials to be an ideal for efficient collection of the charge carriers. The evolution of such materials to be monolithically integrated as a top layer in Si tandem solar cells is exhilarating as the efficiency of such cells approaches 32.5%^[2]. Hence, for the upcoming few decades, the growth of perovskite technology will be in concurrent with the Si technology.

However, despite of such promising accomplishments, perovskites face many challenges in their long-term stability^[3]. The lack of internal stability of such materials and ability to degrade easily with external factors like temperature, pressure, humidity and electric field make the foreseen accomplishments of such structures unproductive. In addition, Si solar cell manufacturers promise a lifetime of almost 25 years, but these issues make the utilization of unstable perovskites in large scale questionable^[4]. Finding suitable external encapsulation for such halide perovskites is of recent research interest, but eventually modifying the internal structure of halide perovskite without affecting its properties is of ultimate importance.

Stable chalcogenides like Cu(In,Ga)Se₂ (CIGS) and other evolving materials like Cu₂ZnSnS₄ (CZTS), Ag₂ZnSnS₄ (AZTS), etc. are promising materials to be a PV absorber but some of the crystallographic factors limits the performance of such materials^[5, 6]. Nevertheless, the stability of such structures are unquestionably superior when compared to that of the halide perovskites. However, such chalcogenides have voltage losses due to the defects present in these materials degrades its promise to be a perfect PV absorber material thus far^[7].

Thus, by effectively combining the advantages of both these technologies i.e. stability from the chalcogenides and defect tolerance with high performance from the halide perovskites, a new promising family of materials chalcogenide perovskites which are chalcogenide materials existing in the perovskite crystal structure is evolved^[8]. Such materials appear to satisfy the key requisites of a highly efficient PV absorber including superior stability and high luminescence^[9]. But manufacturing chalcogenide perovskites and creating uniform films impose few critical challenges like high temperature phase formation and tolerance factor limitations for the existence of perovskite structures. This article discusses in detail some of these key challenges involved in fabrication of such materials. In addition, a small review on the synthesis and performance of the most promising candidate BaZrS₃ to highlight the prospects of these materials is given.

2 Chalcogenide perovskites—structural factors

Like perovskites, chalcogenides perovskites exist in ABX₃ form (where X = S, Se and A, B are metals with a total oxidation state of 6⁺) are quite environmentally safe than lead halide perovskites. According to Tiwari et al.^[10], ABX₃ can crystallise in the desired cubic or pseudo-cubic perovskite structure (types P, N, H, T, and O). The crystal structures of all the five different classes of distorted perovskites are shown in Fig. 1. Out of all the 5 different classes, only type P is distorted perovskite structure but all other structures are non-perovskites.


 (Color online) Possible unit cell structures of chalcogenide perovskites^[10].

Fig. 1. (Color online) Possible unit cell structures of chalcogenide perovskites^[10].

↓ 下载图片

🖼️ 查看所有图片

Not all the metals that satisfy the above condition should form a perovskite structure. But, their ionic radii should satisfy the conditions below^[10]:

$$\text{Tolerance factor } (t) = \frac{r_A + r_X}{\sqrt{2}(r_B + r_X)} \quad (0.7t1.1), \quad \mathbf{1}$$

$$\text{Octahedral factor } (\mu) = \frac{r_B}{r_X} \quad (0.44\mu0.9). \quad \mathbf{2}$$

The tolerance factor is a factor that determines how much the unit cell is distorted. For perfect ABX_3 unit cell, the tolerance factor will be 1. Lower tolerance factor is an indication that distorted perovskite crystal structure with tetragonal, orthorhombic, and rhombohedral structures. Higher tolerance factor ($t > 1.1$) indicates that the cation A is too large for the structure to form stable perovskite^[11].

For oxides, due to the small size of anion ($r_O = 1.40 \text{ \AA}$), the number of possible elements that can form ABO_3 crystal structure with the desired t and μ are very large. But, in case of sulfides and selenides ($r_S = 1.84 \text{ \AA}$ and $r_{Se} = 1.98 \text{ \AA}$) due to the large ionic radii, a relatively large cation can occupy site A to yield desired t , but there are very few possibilities that can yield the desired μ values^[9, 12]. In ABS_3 , heavy alkali cations like Ba^{2+} , Sr^{2+} , and Ca^{2+} are the most suitable candidates for position A and for cation B, Ti, Zr, Hf, Sn are the most optimum candidates due to their stable oxidation state of 4+. Even for all the above combinations, the μ value is below the threshold, a maximum value of 0.39 is observed for $AZrS_3$. Among the suitable cations for A, Ba^{2+} , and Ca^{2+} are the most suitable^[10].

3 Density functional theory (DFT) based calculations on chalcogenide perovskites

Significant results are already pre-exists in studying the stability of various ABX_3 compounds and determining their properties using DFT. Korbel et al.^[13] analysed over 32 000 ABX_3 combinations (oxides, sulfides, selenides) and determined the ground state energies of the compounds through high throughput approach. The calculated energies are found to be much higher than the results obtained elsewhere because he simulated these combinations for a cubic phase with only five atoms and having only one distortion element present. In case of sulfides, Kuhar et al.^[14] study 705 structures with ABS_3 form, but the obtained energy levels are not in agreement with the experimental results. Sophia et al.^[9] has analysed all the reported DFT results and summarized in two different values, H_f is the formation energy of ABX_3 with respect to competing phases and H_g is the formation energy with respect to ground state. They summarized the results using

$$H_f = E_{ABX_3}^{\text{perovskite}} - E_{BX_2} - E_{AX}. \quad \mathbf{3}$$

$$H_g = E_{ABX_3}^{\text{perovskite}} - E_{ABX_3}^{\text{groundstate}}. \quad \mathbf{4}$$

The results reported by them are summarized in Fig. 2. If both H_f and H_g of a material is positive, then ABX_3 structure it leads to will be unstable which makes the synthesis impossible. But, through practice, some of the unstable phases can be obtained, if H_f does not exceed $200 \text{ meV}\cdot\text{f}\cdot\text{u}^{-1}$ and H_g does not exceed $50 \text{ meV}\cdot\text{f}\cdot\text{u}^{-1}$. The difference between these energies, $H_f - H_g$, determines the stability of the ABX_3 ground state against decomposition irrespective of its crystal structure. The structures which are potentially stable according to Sophia et al. are highlighted in green in Fig. 2.



(Color online) Formation energies of chalcogenide perovskite with respect to competing phases (H_f) and ground state formation energy (H_g).

Fig. 2. (Color online) Formation energies of chalcogenide perovskite with respect to competing phases (H_f) and ground state formation energy (H_g).

↓ 下载图片

🖼️ 查看所有图片

According to the above results, for Ba, Sr, and Ca in the site A, Hf and Zr are the identical for B. These structures will be stable according to Sophia et al. and such structures have already been fabricated with ease. So, in this work all the precedent synthesis strategies adopted in fabrication of $BaZrS_3$ is discussed in detail.

4 Properties of $AZrS_3$ (A = Ba, Sr, Ca)

Crystal structures of $BaZrS_3$, $CaZrS_3$, and $SrZrS_3$ are experimentally reported to be $GdFeO_3$ distorted perovskite structure with $pnma$ space group. The Zr atom forms a distorted octahedron with the S atoms, while the A (Ba, Ca, Sr) atoms form a cuboctahedron with the S atoms^[15]. Majumdar et al.^[16] has theoretically predicted the angle of tilting for all the above mentioned perovskite structures. It was reported that for $CaZrS_3$ and $SrZrS_3$, the octahedrons increases on applying the pressure of 15 GPa. But, in contrast, the tilt of octahedron decreases for $BaZrS_3$. The unit cell parameters of the perovskites at various pressures is given in Table 1.

Liu et al.^[17] has theoretically calculated all the photoactive properties of $AZr(SSe)_3$ (Ba, Ca, and Sr). The estimated bandgaps of $AZr(SSe)_3$ structures with varying S and Se ratios are shown in Table 2.

Table 1

Computed unit cell parameters of $AZrS_3$ (A = Ca, Sr, Ba) at 0 and 15 GPa^[16].

System	At 0 GPa			At 15 GPa		
	a	b	c	a	b	c
$CaZrS_3$	7.079.64	6.576.879	166.01			
$SrZrS_3$	7.169.83	6.776.969	416.15			
$BaZrS_3$	7.2710.167	116.959	796.55			

Table 2

Estimated bandgap of various $AZr(SSe)_3$ (A = Ba, Ca, Sr) with varying S, Se ratios^[17].

Compound	E_g (eV)		
	Ba	Ca	Sr
AZrS ₃	1.791	1.981	1.99
AZrS ₂ Se	1.551	1.661	1.66
AZrSSe ₂	1.511	1.521	1.58
AZrSe ₃	1.341	1.401	1.46

Table 3

Electronic properties of AZr(SSe)₃ (A = Ba, Ca, and Sr)^[17].

Compound	m_e^* (m_0)	m_h^* (m_0)	ϵ	E_b (meV)
CaZrS ₃	0.535	0.686	0.30177	
CaZrS ₂ Se	0.571	0.601	0.29367	
CaZrSSe ₂	0.449	0.667	0.26850	
CaZrSe ₃	0.507	0.564	0.26748	
SrZrS ₃	0.522	0.778	0.31285	
SrZrS ₂ Se	0.483	0.581	0.26463	
SrZrSSe ₂	0.523	0.938	0.33671	
SrZrSe ₃	0.516	0.594	0.27753	
BaZrS ₃	0.534	0.849	0.32890	
BaZrS ₂ Se	0.456	0.610	0.26163	
BaZrSSe ₂	0.523	0.938	0.33672	
BaZrSe ₃	0.500	1.097	0.34365	

The bandgap of the structures are found to be increasing as the concentration of S is increasing. Also, comparatively, BaZr(SSe)₃ structures show a much lower bandgap when compared to the Ca and Sr based structures. These results suggests us that bandgap of the structures increases as the ionic radius of A decreases. The band structures shown in Fig. 3 also clearly confirm the direct bandgap of these semiconductors. The maximum absorption coefficient of these structures are observed around $6 \times 10^5 \text{ cm}^{-1}$ suggesting that these structures are most ideal for photovoltaic applications.



(Color online) Band structures for AZrS₃ (A = Ba, Sr, Ca)^[17] (Reproduced with permission from the Royal Society of Chemistry).

Fig. 3. (Color online) Band structures for AZrS₃ (A = Ba, Sr, Ca)^[17] (Reproduced with permission from the Royal Society of Chemistry).

↓ 下载图片

🖼️ 查看所有图片

The partial density of states (PDOS) of AZrS₃ (A = Ba, Sr, Ca) structures are shown in Fig. 4. The top of the valence band arises due to the Zr-4d orbitals while the bottom of the conduction band arises due to the S-3p orbitals. The

contributions of the A atoms are present only on the band edges. The bandgap changes in all these compounds are due to the change in Zr–S bond length in each case.



(Color online) PDOS for AZrS₃ (A = Ba, Sr, Ca)[17] (Reproduced with permission from the Royal Society of Chemistry).

Fig. 4. (Color online) PDOS for AZrS₃ (A = Ba, Sr, Ca)^[17] (Reproduced with permission from the Royal Society of Chemistry).

↓ 下载图片

🖼️ 查看所有图片

The electron and hole effective mass of AZr(SSe)₃ (A = Ba, Ca, and Sr) are shown in the Table 3. These results clearly suggest that the effective mass of the holes are significantly higher when compared to the mass of electrons. Also, the exciton binding energy of these structures decreases as Se increases in the compound.

The formation energies of AZr(SSe)₃ (A = Ba, Ca, and Sr) are shown in the Fig. 5. It is found that selenides are easier to form than the sulfides due to their very low formation energy. These formation energies are calculated by Liu et al. considering that the crystal is at 0 K.



(Color online) Formation energies of AZr(SSe)₃ (A = Ba, Ca, and Sr)[17] (Reproduced with permission from the Royal Society of Chemistry).

Fig. 5. (Color online) Formation energies of AZr(SSe)₃ (A = Ba, Ca, and Sr)^[17] (Reproduced with permission from the Royal Society of Chemistry).

↓ 下载图片

🖼️ 查看所有图片

Meng et al.^[18] conducted an exhaustive investigation into the formation energies and transition energy levels of intrinsic point defects in BaZrS₃. This study is pivotal for identifying growth conditions for the preferential generation of desired beneficial defects while mitigating the deleterious deep-level defects, thereby enhancing the performance characteristics of BaZrS₃ perovskites.

The researchers systematically examined twelve intrinsic point defects, encompassing antisite substitutions, interstitials, vacancies, and cation substitutions. By employing rigorous computational techniques, they determined the transition energies associated with each defect, their respective acceptor-like and donor-like nature, denoted by red and blue highlights, respectively as shown in Fig. 6.



(Color online) Defect energy states for possible defects in BaZrS₃[18] (Reprinted with permission from Meng et al. Copyright [2016] American Chemical Society).

Fig. 6. (Color online) Defect energy states for possible defects in BaZrS₃^[18] (Reprinted with permission from Meng et al. Copyright [2016] American Chemical Society).

↓ 下载图片

🖼️ 查看所有图片

Significantly, among the investigated defects, only five yielded deep-level characteristics: S_{Zr}, S_{Ba}, Zr_S, S_i, and Zr_i. Conversely, the remaining defects act as shallow acceptors or shallow donors. These findings hold considerable significance owing to the profound impact deep-level defects that exert on material performance.

Meng et al. found that near-stoichiometric conditions represent an optimal regime for the synthesis of BaZrS₃ perovskites. Such conditions effectively mitigate the formation of deep-level defects while preserving an appropriate charge carrier density, thereby enhancing the material's overall performance.

Nishigaki et al.^[19] synthesized four different distorted chalcogenide perovskites BaZrS₃, SrZrS₃, BaHfS₃, and SrHfS₃ and also used DFT to calculate the absorption edge of the structures. From Figs. 7(a) and 7(b), the absorption edge of the chalcogenide perovskites is found to be superior to the halide perovskites such as MAPbI₃, GaAs, and CISE. It was concluded that chalcogenide perovskites offer excellent stability and very high absorption when compared to the organic perovskites.



(Color online) (a) Absorption spectra of the chalcogenide perovskites. Open circles represent experimental data and solid lines corresponding to DFT result. (b) Comparison of absorption coefficient of chalcogenide perovskites with traditional PV absorbers^[19] (Reproduced with permission from the John Wiley and sons).

Fig. 7. (Color online) (a) Absorption spectra of the chalcogenide perovskites. Open circles represent experimental data and solid lines corresponding to DFT result. (b) Comparison of absorption coefficient of chalcogenide perovskites with traditional PV absorbers^[19] (Reproduced with permission from the John Wiley and sons).

↓ 下载图片

🖼️ 查看所有图片

Nishigaki et al.^[19] also analysed the performance of BaZr_{0.95}Ti_{0.05}S₃ as a top cell in a perovskite/c-Si tandem cell configuration. A maximum efficiency of 38.7% was achieved which was very high when compared to the halide/perovskite tandem cells constructed before^[20]. A schematic diagram of the device structure and the performance of the tandem cell with respect to thickness is shown in Figs. 8(a)–8(c).



(Color online) (a) Structure of perovskite/c-Si tandem cell. (b) Quantum efficiency of top and bottom cell. (c) Variation of efficiency with respect to thickness of the perovskite^[19] (Reproduced with permission from the John Wiley and sons).

Fig. 8. (Color online) (a) Structure of perovskite/c-Si tandem cell. (b) Quantum efficiency of top and bottom cell. (c) Variation of efficiency with respect to thickness of the perovskite^[19] (Reproduced with permission from the

John Wiley and sons).

↓ 下载图片

🖼 查看所有图片

5 BaZrS₃

Already BaZrS₃ is synthesized through techniques like pulsed laser deposition, nanoparticles based approach, solid state reaction, chemical vapour deposition etc., till now. But, all these synthesis routes involve formation of BaZrS₃ through either of the two reactions given below.

From the sulfide precursors,



From the oxide precursors

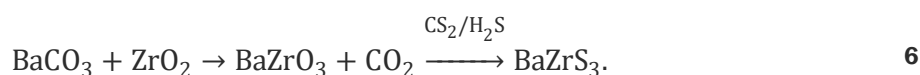


Table 4

Reported synthesis strategies adopted for synthesis of BaZrS₃.

S.No.	Author	Synthesis route	Outcomes
1	Hahn and Mutschke [21]	Binary sulphides reaction at a very high synthesis temperature	Ternary BaZrS ₃ formed at the boundary of two binary phases, hinder further formation of the ternary phase.
2	Leleiveld et al. [22]	Sulfurize a mixture of BaCO ₃ and ZrO ₂ in H ₂ S environment at 1373 K	Formation of BaZrS ₃ having a structure identical to gadolinium orthoferrite upon annealing for 24 h.
3	Clearfield et al. [23]	Sulfurization	Temperatures from 950 to 1200°C at various time periods from 4 to 24 h.
4	Niu et al. [25]	Solid state reaction	Iodine was used to catalyze the reaction and reduce the synthesis time.
5	Xu et al. [26]	Improved sulfurization	A new sulfurization technique to raise the chemical potential of technique and the conversion CS ₂ is used. rate was proposed as an indicator of the sulfurization level
6	Wei et al. [27]	Ball milling, followed by sulfurization	Synthesized Ti alloyed Ba(Zr _{1-x} Ti _x)S ₃ powders with x from 0 to 0.1. Structural integrity of the distorted chalcogenide phase is retained till 4%.

S.No.	Author	Synthesis route	Outcomes
7	Sharma et al. [28]	Ti-alloyed BaZrS ₃ films were obtained by sulfurization of Ti-as carrier gas alloyed BaZrO ₃ films	BaZrO ₃ films were sulfurized in a 3 zone furnace with CS ₂ and N ₂
8	Ravi et al. ^[30]	Solid-state synthesis	BaZrS ₃ NCs are first prepared using a solid-state synthesis route, and the subsequent surface modifications lead to a colloidal dispersion of NCs in both polar N-methyl-2-pyrrolidinone and non-polar chloroform solvents.
9	Yu et al. ^[32]	Pulsed laser deposition of a BaZrS ₃ target	Synthesis of BaZrS ₃ thin films at temperatures as low as 500 °C, this is achieved by changing the chemical reaction pathway from sulfurization of oxide perovskites to crystallization of pulsed laser deposited amorphous BaZrS _x films.
10	Comparatto et al. ^[33]	Sputtering, Ba–Zr precursor films capped by SnS, sulfurized at under 600 °C for 20 min	The partial pressure of sulfur was found to be the key factor in determining the diffusion and crystallization of the precursors.
11	Pradhan et al. [34]	Solution processing	With a sulfurization at 575 °C for 20 min, the molecular precursors converted into single phase thin films. Increasing sulfurization time results in more intense and higher energy photoluminescence emissions.
12	Vincent et al. [35]	Solution processing	High-quality thin films of large-grain BaZrS ₃ perovskites are prepared by solution processing at moderate temperatures. The study discovered that a barium polysulfide liquid flow is crucial for the fast synthesis of the perovskite, and this method was effectively applied to the BaHfS ₃ perovskite as well.
13	Ramanandan et al. ^[36]	Two-step synthesis mechanism of BaZrS ₃ , involving an intermediary amorphization phase of BaZrO ₃	They identify sulfur species diffusion within the film as the rate-determining step. The conversion of H ₂ S to the sulfide phase varies significantly with processing temperature.
14	Dhole et al. ^[37]	Polymer-assisted deposition	This technique involved the deposition of cation precursor films chelated with polymer, followed by sulfurization in a mixed atmosphere of carbon disulfide and argon.
15	Romagnoli et al. ^[38]	Simple synthetic approach under relatively mild conditions (T = 500 °C) and is complete in a few hours	By combining BaS, Zr(Hf), and S powders for 20 min in mortar and pestle and sulfurization.

Even though these equations make it easy to see how BaZrS₃ is made, it is hard to make high-quality BaZrS₃ because it grows poorly at temperatures above 1000 °C and takes many hours or days to respond. These unconventional conditions make the PV devices formation extremely challenging. These challenging synthesis conditions might be due to the following reasons.

Several studies confirmed that formation of BaZrS₃ by reaction of binary sulphides demand a very high synthesis temperature. For example, Hahn and Mutschke^[21] discovered that even though the ternary BaZrS₃ phase is more stable than the binary ZrS₂ and BaS, but these two phases does not react until 900 °C. They also concluded that the ternary BaZrS₃ formed at the boundary of two binary phases, hindering further formation of the ternary phase because it reduces the diffusion of the precursors and a lot of thermal energy is required to overcome this kinetic diffusion barrier.

Another strategy for synthesizing BaZrS₃ is to sulfurize a mixture of BaCO₃ and ZrO₂ in H₂S environment. But, this process also demands a synthesis temperatures of 1373 K. Leleiveld et al.^[22] utilized this route to synthesize BaZrS₃ but the sulfurization was carried for seven days. Neutron diffraction results reveal the formation of BaZrS₃ having a structure identical to gadolinium orthoferrite (GdFeO₃). The estimated lattice parameters for the structures are found to be (a, b, c) = (0.70599, 0.99813, 0.70251 nm) with a space group of Pnma and Z = 4. Using the same route, Clearfield et al.^[23] fabricated BaZrS₃ at temperatures from 950 to 1200 °C at various time periods from 4 to 24 h. Structural characterizations revealed the lattice parameters as (a, b, c) = (0.7037, 0.9983, 0.7050 nm) and they exhibited a distorted perovskite structure.

Using first principles calculation, Sun et al.^[24] has evaluated the optoelectronic properties of various ABX₃ compounds, where A represents a 2+ cation and B denotes a 4+ cation and X is either sulphur or selenium. They also estimated the bandgap of the structures. From these structures, they have discovered that BaZrS₃, CaHfSe₃, CaZrSe₃, and CaTiS₃ will be ideal for photovoltaic applications owing to their optimal bandgap and very high absorption coefficient greater than 10⁵ cm⁻¹.

The major advantage of such structures was long term stability and ability to tolerate heat up to 400 °C. In order to understand that, Niu et al.^[25] synthesized and evaluated the thermal stability of BaZrS₃, Ba₂ZrS₄, α-SrZrS₃, β-SrZrS₃, and Ba₃Zr₂S₇. By studying differential scanning calorimetry and thermogravimetric analysis (DSC-TGA) of such structures, they proved that perovskite chalcogenides are highly stable in air up to a temperature of 550 °C.

Xu et al.^[26] studied the thermal stability of BaZrS₃ by heat treating at air and at very low pressure. They concluded that BaZrS₃ was stable till 400 °C in air and in a low pressure of 10⁻¹ Pa, it was stable till 700 °C. These results are crucial to understand the stability of such structures under post deposition treatments that may be essential during the fabrication of photovoltaic devices with BaZrS₃.

The bandgap of BaZrS₃ can be tuned by alloying with various elements like Ti, Hf, etc. In order to study the effects of Ti alloying on BaZrS₃, Wei et al.^[27] synthesized Ba(Zr_{1-x}Ti_x)S₃ powders with varying x values between 0 and 0.1. By alloying 4% of Ti into BaZrS₃, the bandgap can be lowered to 1.51 eV from 1.78 eV. This reduction in bandgap can lead to significant increase in the solar cell efficiency. Structural integrity of the distorted chalcogenide phase is

retained till 4%, but while doping at higher concentration, the structure is observed to destabilize and binary sulphides tend to form. This study on band gap tailoring using Ti-alloying of BaZrS₃ is unique as it drives BaZrS₃ towards the solar cell based devices.

A similar strategy was utilized by Sharma et al.^[28] in obtaining Ti alloyed BaZrS₃ films using chemical vapour deposition method. They observed that upon 6% Ti alloying, the bandgaps lowered from 1.75 to 1.4 eV, which is the most optimum bandgap corresponding to the Shockley–Queisser limit. Alloying concentrations above 6% lead to degradation of the disordered perovskite phase and phase segregation which is in agreement with their theoretical results too. Titanium-alloyed BaZrS₃ thin films can serve as an excellent option for optoelectronic devices because of their ideal bandgap, great environmental stability, and non-toxic behaviour.

The stability of photodetectors fabricated using BaZrS₃ and MAPbI₃ was computed and calculated by Gupta et al.^[29]. They observed that upon operation in humid environments, organic perovskite's photoresponsivity degraded by 95% in four weeks, while the inorganic perovskite BaZrS₃ retained 60% of the initial performance. This shows that chalcogenide perovskites degrade at a much slower rate which is due to the very low anion migration rate in them when compared to MAPbI₃. The discovery provides both theoretical reasoning and experimental evidence supporting the environmental viability of BaZrS₃. This chalcogenide perovskite emerges as a highly promising candidate for optoelectronics due to its notable absence of toxic lead and inherent sustainability.

Cubic BaZrS₃ nanocrystals of edge lengths between 40 and 60 nm are synthesized by Ravi et al.^[30] through solid-state synthesis. The structural stability of the nanostructures is investigated through XRD and XAFS (X-ray absorption fine structure) at temperatures between 15 and 613 K. They also tuned the surface chemistry of the nanostructures to make a stable colloidal suspension in polar solvent (N-methyl-2-pyrrolidinone) as well as the non-polar solvent (chloroform). Spin coated thin films of the colloids are fabricated and the hole mobility of 0.059 cm²·V⁻¹·s⁻¹ and electron mobility of 0.017 cm²·V⁻¹·s⁻¹ are found and the nanocrystals show both p and n type ambipolar transistors behaviour.

Pulsed laser deposited amorphous BaZrO₃ precursors are sulfurized by Márquez et al.^[31] in 5% H₂S + Ar mixture at temperatures from 700 to 1100 °C for 30 min to obtain BaZrS₃–BaZrO₃ perovskite films. S concentration in the films is found to be increasing as the sulfurization temperature is increased signifies the incorporation of S into BaZrO_x. The photographs, FESEM images and XRD patterns of the films are shown in Figs. 9(a)–9(c).



(Color online) (a) Photographs, (b) surface morphology, and (c) XRD patterns of the BaZrS₃ films prepared at various sulfurization temperatures^[31] (Reprinted with permission from Marquez et al. Copyright [2021] American Chemical Society).

Fig. 9. (Color online) (a) Photographs, (b) surface morphology, and (c) XRD patterns of the BaZrS₃ films prepared at various sulfurization temperatures^[31] (Reprinted with permission from Marquez et al. Copyright [2021] American Chemical Society).

↓ 下载图片

🖼️ 查看所有图片

Also, the S incorporation saturates at temperatures above 1000 °C and through this route a maximum S/(S + O) ratio of 0.85 is achieved showing that the oxide phase is preserved in the thin film in a trace amount.

Amorphous BaZrS₃ films were prepared using pulsed laser deposition of a BaZrS₃ target by Yu et al.^[32] The films are crystallized by processed in CS₂ at temperatures varying from 500 to 900 °C. Phase purity was observed in all the films and specifically at 550 °C the films were highly crystalline with very low surface roughness less than 0.6 nm. They also developed prototype photodetector systems and FET devices using the fabricated BaZrS₃ films.

Through sputtering, Ba–Zr precursor films capped by SnS were synthesized by Comparatto et al.^[33] and sulfurized at under 600 °C for 20 min. The partial pressure of sulfur was found to be the key factor in determining the diffusion and crystallization of the precursors. Although, presence of trace Sn was observed in the films, but the crystallinity of the films was found to be superior. This study also emphasized the importance of a capping layer SnS on the Ba–Zr precursors which prevented the Ba–Zr films from oxidation.

Through solution processing Pradhan et al.^[34] synthesized BaZrS₃ and BaHfS₃ films. With a sulfurization at 575 °C for 20 min, the molecular precursors converted into single phase thin films. This accomplishment not only reduced the sulfurization temperature multifold. This process significantly eased the fabrication challenges that were faced by the research community.

Vincent et al.^[35] used a solution processing approach to understand the underlying mechanism and develop methodologies for producing high-quality thin films of large-grain BaZrS₃ perovskites at moderate temperatures. The study discovered that a barium polysulfide liquid flow is crucial for the fast synthesis of the perovskite, and this method was effectively applied to the BaHfS₃ perovskite as well. The findings provide information on precursor choice, sulfurization temperature ranges, and reaction conditions that are likely to promote the development of large-grain chalcogenide perovskite, which is critical for producing device-grade thin films.

Ramanandan et al.^[36] elucidated the two-step synthesis mechanism of BaZrS₃, involving an intermediary amorphization phase of BaZrO₃. They identify sulfur species diffusion within the film as the rate-determining step. The conversion of H₂S to the sulfide phase varies significantly with processing temperature. Despite Zr-rich precursors, stoichiometric BaZrS₃ (1 : 1 : 3) predominates, accompanied by ZrO₂ as a secondary phase, in contrast to the versatile non-stoichiometric compositions observed in chalcopyrites and kesterites. BaZrS₃ stands out from other chalcogenides in this aspect. The findings of this study pave the way for further optimization of BaZrS₃ synthesis processes, thereby expanding the potential applications of this material in the future.

Dhole et al.^[37] effectively fabricated thin films of BaZrS₃ utilizing a polymer-assisted deposition (PAD). This technique involved the deposition of cation precursor films chelated with polymer, followed by sulfurization in a mixed atmosphere of carbon disulfide and argon. Through X-ray diffraction (XRD) and Raman spectroscopy analyses, the study confirmed the formation of single-phase polycrystalline BaZrS₃ thin films at 900 °C. These BaZrS₃ films exhibited a photoluminescence peak at approximately 1.80 eV and demonstrated the capability to generate a photogenerated current upon light illumination at a wavelength of 530 nm.

Romagnoli et al.^[38] produced BaZrS₃ by combining BaS, Zr(Hf), and S powders in a 1 : 1 : 3 molar ratio in an agate mortar for 20 min in air. The powder was then transported through a sealed ampoule and heated in a muffle furnace at 500 °C overnight to produce phase pure BaZr_xHf_{1-x}S₃ nanoparticles. The ability to change the band gap of the material from 1.78 to 2.11 eV by adjusting the Hf/Zr ratio is fascinating. The precedent literatures discussed in this article are summarized in Table 4.

6 Predicted device structures using SCAPS-1D simulator

Till now no experimental reports on application of BaZrS₃ is reported, but in recent times many reports towards identifying various constituent materials that are most optimal for the BaZrS₃ photovoltaic devices using SCAPS-1D are available. Mercy et al.^[39] has clearly summarized all the precedent literatures and their reported configurations and device performances. The photovoltaic device performances of all the precedent literatures are summarized in Table 5.

Among all the configurations reported till now, FTO/ZrS₂/BaZrS₃/SnS/Pt device configuration is reported to be more appropriate. A maximum efficiency of 28.17% was reported which was very close to the theoretical maximum efficiency of 30.17% for BaZrS₃ perovskite^[45]. So, the experimental researches can use this structure for their initial fabrication of devices.

Table 5

Reported solar cell device structures for BaZrS₃ photovoltaics.

Device Structure	Estimated solar cell characteristics				Reference
	V _{oc} (V)	J _{sc} (mA/cm ²)	FF	Efficiency (%)	
FTO/TiO ₂ /BaZrS ₃ /Spiro-OMeTAD/Au	1.21	16.54	86.26	17.29	[40]
FTO/TiO ₂ /BaZrS ₃ /Cu ₂ O/Au	1.16	12.24	87.13	12.42	[41]
FTO/TiO ₂ /BaZrS ₃ /CuSbS ₂ /W	1.00	22.57	73.7	17.13	[42]
FTO/TiO ₂ /BaZrS ₃ /Spiro-OMeTAD/Au	0.70	22.00	79.40	12.12	[43]
AZO/i-ZnO/CdS/BaZrS ₃ /a-Si	1.31	19.08	78.88	19.72	[44]
FTO/TiO ₂ /BaZrSe ₃ /Spiro-OMeTAD/Au	0.72	46.65	77.32	25.84	[43]
FTO/TiO ₂ /Ba(Zr _{0.87} ,Ti _{0.12})S ₃ /Cu ₂ O/back contact	1.09	26.57	85.78	24.86	[27]
AZO/i-ZnO/CdS/Ba(Zr _{0.95} ,Ti _{0.05})S ₃ /a-Si	1.26	27.06	88.47	30.06	[44]
FTO/ZrS ₂ /BaZrS ₃ /SnS/Pt	1.18	29.74	80.15	28.17	[39]
FTO/ZrS ₂ /Ba(Zr _{0.96} ,Ti _{0.04})S ₃ /SnS/ Pt	1.18	32.26	84.94	32.58	[39]

7 Conclusions and future scope

Till now the precedent literatures discussed shows promise on reducing the synthesis of BaZrS₃, but no photovoltaic devices are constructed till now. This is majorly due to the lack of knowledge of the proper solar cell structure that is needed. Many simulation studies already showed promising cell structures similar to that of CZTS, but a practical

analysis of such photovoltaic devices are yet to be studied in detail. Also, the defect engineering, bandgap gradient structures and post deposition annealing which are promising strategies in CIGS and CZTS based devices can be adopted here.

Potential synthesis routes need to be identified to fabricate BaZrS_3 at low temperature through solution processed techniques. This can lead to fabrication of BaZrS_3 over flexible photovoltaic applications. Along with BaZrS_3 , other potential chalcogenide perovskites need to be researched for their photovoltaic performance which can enlighten the stability and usefulness of these structures in energy conversion. Also, possibilities of integrating these perovskites into tandem structures with other promising photovoltaic technologies can be a potential area of research.

References

[1] Yoo J J, Seo G, Chua M Ret al Efficient perovskite solar cells via improved carrier management Nature 2021 590:58710.1038/s41586-021-03285-w

[2] Mariotti S, Köhnen E, Scheler Fet al Interface engineering for high-performance, triple-halide perovskite-silicon tandem solar cells Science 2023 381:6310.1126/science.adf5872

[3] Wang Q, Phung N, Di Girolamo Det al Enhancement in lifespan of halide perovskite solar cells Energy Environ Sci 2019 12:86510.1039/C8EE02852D

[4] Xie H B, Lira Cantu M Multi-component engineering to enable long-term operational stability of perovskite solar cells J Phys Energy 2020 24:00810.1088/2515-7655/ab8278

[5] Kannan P K, Anandkumar M A theoretical investigation to boost the efficiency of CZTS solar cells using SCAPS-1D Optik 2023 288:17121410.1016/j.ijleo.2023.171214

[6] Wang L, Liu R J, Luan H Met al The enhancement of CZTSSe solar cell performance through active construction of the double-layer absorber Sol Energy Mater Sol Cells 2024 266:11267010.1016/j.solmat.2023.112670

[7] Keller J, Kiselmann K, Donzel Gargand O et al High-concentration silver alloying and steep back-contact gallium grading enabling copper indium gallium selenide solar cell with 23.6% efficiency Nat Energy 2024 9:46710.1038/s41560-024-01472-3

[8] Jeong A R, Choi S B, Kim W Met al Electrical analysis of c-Si/CGSe monolithic tandem solar cells by using a cell-selective light absorption scheme Sci Rep 2017 7:1572310.1038/s41598-017-15998-y

[9] Sopiha K V, Comparotto C, Márquez J A et al Chalcogenide perovskites: Tantalizing prospects, challenging materials Adv Optical Mater 2022 10:210170410.1002/adom.202101704

[10] Tiwari D, Hutter O S, Longo G Chalcogenide perovskites for photovoltaics: Current status and prospects J Phys

Energy2021303401010.1088/2515-7655/abf41c

[11] Shannon R D Revised effective ionic radii and systematic studies of interatomic distances in halides and chalcogenides *Acta Crystallogr Sect A* 1976 32 75 110.1107/S0567739476001551

[12] Pilania G, Ghosh A, Hartman S Tet al Anion order in oxysulfide perovskites: Origins and implications *NPJ Comput Mater* 2020 6 7 110.1038/s41524-020-0338-1

[13] Körbel S, Marques M A L, Botti S Stability and electronic properties of new inorganic perovskites from high-throughput ab initio calculations *J Mater Chem C* 2016 4 3 15 710.1039/C5TC04172D

[14] Kuhar K, Crovetto A, Pandey Met al Sulfide perovskites for solar energy conversion applications: Computational screening and synthesis of the selected compound LaYS₃ *Energy Environ Sci* 2017 10 25 79 10.1039/C7EE02702H

[15] Adjogri S J, Meyer E L Chalcogenide perovskites and perovskite-based chalcogenide as photoabsorbers: A study of their properties, and potential photovoltaic applications *Materials* 2021 14 7 85 7 10.3390/ma14247857

[16] Majumdar A, Adeleke A A, Chakraborty Set al Emerging piezochromism in lead free alkaline earth chalcogenide perovskite AZrS₃ (a = Mg, Ca, Sr and Ba) under pressure *J Mater Chem C* 2020 8 16 39 2 10.1039/D0TC04516K

[17] Liu D W, Zeng H H, Peng Het al Computational study of the fundamental properties of Zr-based chalcogenide perovskites for optoelectronics *Phys Chem Chem Phys* 2023 25 13 75 5 10.1039/D3CP01522J

[18] Meng W W, Saporov B, Hong Fet al Alloying and defect control within chalcogenide perovskites for optimized photovoltaic application *Chem Mater* 2016 28 8 2 110.1021/acs.chemmater.5b04213

[19] Nishigaki Y, Nagai T, Nishiwaki Met al Extraordinary strong band-edge absorption in distorted chalcogenide perovskites *Sol RRL* 2020 4 20 7 005 110.1002/solr.202070051

[20] Sahli F, Werner J, Kamino B A et al Fully textured monolithic perovskite/silicon tandem solar cells with 25.2% power conversion efficiency *Nat Mater* 2018 17 8 20 10.1038/s41563-018-0115-4

[21] Hahn H, Mutschke U Untersuchungen über ternäre Chalkogenide. XI. Versuche zur Darstellung von Thioperovskiten *Z Für Anorg Und Allg Chem* 1957 288 269 10.1002/zaac.19572880505

[22] Lelieveld R, IJdo D J W Sulfides with the GdFeO₃ structure *Acta Crystallogr Sect B* 1980 36 2 22 3 10.1107/S056774088000845X

[23] Clearfield A The synthesis and crystal structures of some alkaline earth titanium and zirconium sulfides *Acta Crystallogr* 1963 16 13 5 10.1107/S0365110X6300030X

[24] Sun Y, Agiorgousis M L, Zhang P. Heterostructure of chalcogenide perovskites for photovoltaics. *Nano Lett* 2015;15(8):110.1021/nl504046x

[25] Niu S Y, Milam-Guerrero J, Zhou Y. Thermal stability study of transition metal perovskite sulfides. *J Mater Res* 2018;34(13):1557-1567. doi:10.1557/jmr.2018.419

[26] Xu J, Fan Y C, Tian W. Enhancing the optical absorption of chalcogenide perovskite BaZrS₃ by optimizing the synthesis and post-processing conditions. *J Solid State Chem* 2022;307:122872. doi:10.1016/j.jssc.2021.122872

[27] Wei X C, Hui H L, Perera S. Ti-alloying of BaZrS₃ chalcogenide perovskite for photovoltaics. *ACS Omega* 2020;5(18):18579-18587. doi:10.1021/acsomega.0c00740

[28] Sharma S, Ward Z, Bhimani K. Bandgap tuning in BaZrS₃ perovskite thin films. *ACS Appl Electron Mater* 2021;3(3):306-310. doi:10.1021/acsaelm.1c00575

[29] Gupta T, Ghoshal D, Yoshimura A. An environmentally stable and lead-free chalcogenide perovskite. *Adv Funct Mater* 2020;30(20):2001387. doi:10.1002/adfm.202001387

[30] Ravi V K, Yu S H, Rajput P. Colloidal BaZrS₃ chalcogenide perovskite nanocrystals for thin film device fabrication. *Nanoscale* 2021;13(16):1610-1619. doi:10.1039/D0NR08078K

[31] Márquez J A, Rusu M, Hempel H. BaZrS₃ chalcogenide perovskite thin films by H₂S sulfurization of oxide precursors. *J Phys Chem Lett* 2021;12(21):4810-4815. doi:10.1021/acs.jpcclett.1c00177

[32] Yu Z H, Wei X C, Zheng Y. Chalcogenide perovskite BaZrS₃ thin-film electronic and optoelectronic devices by low temperature processing. *Nano Energy* 2021;85:105959. doi:10.1016/j.nanoen.2021.105959

[33] Comparotto C, Ström P, Donzel G. Synthesis of BaZrS₃ perovskite thin films at a moderate temperature on conductive substrates. *ACS Appl Energy Mater* 2022;5(6):335-340. doi:10.1021/acsaem.2c00704

[34] Pradhan A A, Uible M C, Agarwal S. Synthesis of BaZrS₃ and BaHfS₃ chalcogenide perovskite films using single-phase molecular precursors at moderate temperatures. *Angew Chem Int Ed* 2023;62(202301049):10.1002/anie.202301049

[35] Vincent K C, Agarwal S, Turnley J. Liquid flux-assisted mechanism for modest temperature synthesis of large-grain BaZrS₃ and BaHfS₃ chalcogenide perovskites. *Adv Energy Sustain Res* 2023;4(2):3000-3010. doi:10.1002/aesr.202300010

[36] Ramanandan S P, Giunto A, Stutz E Z et al. Understanding the growth mechanism of BaZrS₃ chalcogenide perovskite thin films from sulfurized oxide precursors. *J Phys Energy* 2023;50(14):01310.1088/2515-7655/aca9fe

[37] Dhole S, Wei X C, Hui H L et al. A facile aqueous solution route for the growth of chalcogenide perovskite BaZrS₃ films. *Photonics* 2023;10(3):36610.3390/photronics10040366

[38] Romagnoli L, Ciccio A, Dale P J et al. A simple synthetic approach to BaZrS₃, BaHfS₃, and their solid solutions. *J Am Ceram Soc* 2024;107(6):9810.1111/jace.19506

[39] Vincent Mercy E N, Srinivasan D, Marasamy L. Emerging BaZrS₃ and Ba(Zr, Ti)S₃ chalcogenide perovskite solar cells: A numerical approach toward device engineering and unlocking efficiency. *ACS Omega* 2024;9(43):5910.1021/acsomega.3c06627

[40] Najwa C, Mustapha R, Boubker F. Numerical study of BaZrS₃ based chalcogenide perovskite solar cell using SCAPS-1D device simulation, 2022, PREPRINT (Version 1) available at Research Square [<https://doi.org/10.21203/rs.3.rs-1251663/v1>]

[41] Karthick S, Velumani S, Bouclé J. Chalcogenide BaZrS₃ perovskite solar cells: A numerical simulation and analysis using SCAPS-1D Opt. *Mater* 2022;126(11):225010.1016/j.optmat.2022.112250

[42] Goutham Kumar S, Pramod A, Prashanth C R et al. Proposal for a novel perovskite solar cell based on BaZrS₃ with optimized electron and hole transport layer using SCAPS-1D. *Eur Chem Bull* 2023;12(10):289

[43] Kumar P, Sharma P. Design and simulation of chalcogenide perovskite BaZr(S, Se)₃ compositions for photovoltaic applications. *Phys Scr* 2023;98(06):592110.1088/1402-4896/acfc6

[44] Barman B, Ingole S. Analysis of Si back-contact for chalcogenide perovskite solar cells based on BaZrS₃ using SCAPS-1D. *Adv Theory Simul* 2023;6(2):20082010.1002/adts.202200820

[45] Rühle S. Tabulated values of the Shockley-Queisser limit for single junction solar cells. *Sol Energy* 2016;130(1):3910.1016/j.solener.2016.02.015

☰ 论文摘要

📄 Full Text

📊 图 & 表

⊕ 补充材料

ⓘ 基本信息

🔍 知识挖掘

📈 Metrics

📄 PDF全文

参考文献 & 引文

引用该论文: TXT | EndNote

被引通知

PDF全文



相关论文



相关资讯



